



The Effects of AlF₃ Coating on the Performance of Li[Li_{0.2}Mn_{0.54}Ni_{0.13}Co_{0.13}]O₂ Positive Electrode Material for Lithium-Ion Battery

J. M. Zheng,^a Z. R. Zhang,^{a,b} X. B. Wu,^a Z. X. Dong,^a Z. Zhu,^b and Y. Yang^{a,*}

^aState Key Laboratory for Physical Chemistry of Solid Surfaces, Department of Chemistry, College of Chemistry and Chemical Engineering and ^bDepartment of Physics, Xiamen University, Xiamen 361005, People's Republic of China

AlF₃-coated Li[Li_{0.2}Mn_{0.54}Ni_{0.13}Co_{0.13}]O₂ materials have been synthesized as positive electrode materials for lithium-ion batteries. The pristine and AlF₃-coated Li[Li_{0.2}Mn_{0.54}Ni_{0.13}Co_{0.13}]O₂ materials were characterized by X-ray diffraction, scanning electron microscopy, differential scanning calorimetry, and charge-discharge techniques. The electrochemical studies indicated that the AlF₃-coated Li[Li_{0.2}Mn_{0.54}Ni_{0.13}Co_{0.13}]O₂ showed initial irreversible capacity loss of only 47 mA h/g compared to 75.5 mA h/g for pristine material. Meanwhile, the coated material also exhibited better rate capability and cyclic performance, which has higher capacity retention of 87.9% after 80 cycles at 0.5 C rate at room temperature in comparison with only 67.8% for the pristine one. The functional mechanism of AlF₃ coating on the performance of Li[Li_{0.2}Ni_{0.13}Mn_{0.54}Co_{0.13}]O₂ was also investigated by electrochemical impedance spectroscopy (EIS) and in situ differential electrochemical mass spectrometry (DEMS). EIS analysis indicated that AlF₃-coated Li[Li_{0.2}Mn_{0.54}Ni_{0.13}Co_{0.13}]O₂ had stable charge transfer resistance (*R*_{ct}). In situ DEMS results revealed that the activity of extracted oxygen species from layered positive electrode material was greatly reduced and the decomposition of the electrolyte was significantly suppressed for AlF₃-coated Li[Li_{0.2}Mn_{0.54}Ni_{0.13}Co_{0.13}]O₂. Therefore, more oxygen molecules rather than carbon dioxide were observed in the coated material system. It is demonstrated again that the AlF₃ coating layer played an important role in the stabilization of the electrode/electrolyte interface for the coated material.
© 2008 The Electrochemical Society. [DOI: 10.1149/1.2966694] All rights reserved.

Manuscript submitted April 14, 2008; revised manuscript received July 9, 2008. Published August 25, 2008.

The search for cheaper, higher capacity, and safer layered-positive electrode materials to substitute for LiCoO₂ has been one of the most important subjects in the study of electrode materials for high energy density Li-ion battery. With this aim, many positive-electrode materials have been developed for advanced lithium-ion batteries.¹ In recent years, layered LiMn_{1/2}Ni_{1/2}O₂ and LiMn_{1/3}Ni_{1/3}Co_{1/3}O₂ have attracted much attention as improved positive electrodes due to the merits of Mn-containing electrode materials.²⁻⁵ It has also been shown that the addition of extra lithium, manganese, and charge-compensating oxygen into LiMn_{1/2}Ni_{1/2}O₂ and LiMn_{1/3}Ni_{1/3}Co_{1/3}O₂ results in the formation Li₂MnO₃-like regions or domains that are structurally integrated into LiMn_{1/2}Ni_{1/2}O₂ and LiMn_{1/3}Ni_{1/3}Co_{1/3}O₂ components.⁶⁻⁸ The Li₂MnO₃ component is proposed and demonstrated to stabilize the composite electrode structure, and results in enhancement of the discharge capacity of the electrode by extracting the lithium concomitant with the release of oxygen (a net loss of Li₂O) at high potential such as 4.6–4.8 V.⁶ In addition, recent advances of the Li₂MnO₃-based positive electrode materials such as *x* Li₂MnO₃·(1 - *x*) LiMO₂ (*M* = Mn, Ni, Co, or combinations) have been highlighted in the feature article reported by Thackeray et al.⁹ Recently, the series compounds *x* Li₂MnO₃·(1 - *x*) LiNi_{1/3}Co_{1/3}Mn_{1/3}O₂ have been reported to be very promising by Johnson et al.⁶ and Wu et al.¹⁰ because of their high capacities. As reported by Johnson, an anomalously high capacity in excess of the theoretical value, typically 280–300 mA h/g was obtained if a low current rate (0.05 mA/cm²), an elevated temperature (50°C), and a relatively high value of *x* (0.5 and 0.7) were used. For example, the positive electrode Li[Li_{0.2}Mn_{0.54}Ni_{0.13}Co_{0.13}]O₂, which can be re-written in two-component notation as 0.5 Li₂MnO₃·0.5 LiNi_{1/3}Co_{1/3}Mn_{1/3}O₂ (*x* = 0.5), could deliver an initial discharge capacity of 286 mA h/g under the above-mentioned conditions.

Although solid solutions between Li₂MnO₃ and LiMO₂ were reported to deliver high initial discharge capacities in excess of 200 mA h/g, the electrode materials must be charged to considerably high potentials of 4.6 or 4.8 V, which are beyond the electrochemical stable window of the normal electrolytes widely used

nowadays. It has been shown by some authors that potentials in excess of 4.2–4.5 V are high enough to oxidize the alkyl carbonates.¹¹ As reported by Robertson and Bruce,¹² in addition to hydrolysis of electrolytes with a trace amount of water, the oxidation of the alkyl carbonates would also lead to the generation of H⁺ and thus resulted in increase of acidity of the electrolyte. The X-ray photoelectron spectroscopy measurements on the charged Li₂MnO₃ materials did reveal the presence of significant quantities of carbon containing compounds and lithium fluoride on the surface of the charged electrode. Thus, oxidation of electrolytes at high potentials and the attack of acidic species (HF) would lead to damage and/or degradation of the electrode/electrolyte interface on the electrodes and result in deteriorated electrochemical performance of the materials on extensive cycling.

Furthermore, the extensive removal of Li⁺ concomitant with the extraction of oxygen (Li₂O) during the activation process also appears to damage the electrode surface during electrochemical activation because the cell impedance increases and the capacity declines steadily on cycling, particularly when higher current rates are applied. This is apparent in the material with a formula 0.1 Li₂MnO₃·0.9 LiNi_{0.256}Co_{0.372}Mn_{0.372}O₂ as reported in Ref. 9, which showed a relatively rapid decline in capacity on cycling (3.0–4.6) when current density was increased fivefold after the two initial cycles.

Many strategies have been directed to ameliorate cycling stability of the lithium-rich positive electrode materials. The experimental data reported by Kang and Amine¹³ showed that fluorine substitution significantly enhanced the cycling performance of the pristine Li[Li_{0.2}Mn_{0.55}Ni_{0.15}Co_{0.10}]O₂ material despite not disclosing the reason. Kang and Thackeray¹⁴ also reported that preconditioned 0.1 Li₂MnO₃·0.9 LiNi_{0.256}Co_{0.372}Mn_{0.372}O₂ electrode powders with mildly acidic fluoride solutions such as 2.4 × 10⁻³ M NH₄PF₆ or (NH₄)₃AlF₆ and NH₄BF₄ led to remarkable cycling stability of both lithium half-cells and full lithium ion cells, in comparison with the electrochemical performance of the untreated electrode.

Surface modification has also been shown to be a facile and useful approach to improve the electrochemical performance of positive electrode materials when they are charged to a high cut-off potential. For example, Al(OH)₃-coated Li[Li_{0.2}Ni_{0.2}Mn_{0.6}]O₂ material has shown to have a better rate capability and thermal stability compared to the pristine system.¹⁵ In addition, surface-modified

* Electrochemical Society Active Member.

^z E-mail: yyang@xmu.edu.cn

layered-Li[Li_{(1-x)/3}Mn_{(2-x)/3}Ni_{x/3}Co_{x/3}]O₂ electrodes with Al₂O₃ have also been proven to be with lower irreversible capacity loss in comparison with the pristine ones.¹⁰ Myung et al.¹⁶ also verified that the amphoteric Al₂O₃ coating layer can scavenge the trace acidic HF species from the electrolyte by time of flight-secondary-ion mass spectrometry. However, some of the Al₂O₃ coating layer will gradually convert to AlF₃ after extended cycling, suggesting that the amphoteric Al₂O₃ coating layer is not endurable from the HF attack in the electrolyte. Therefore, more recently, AlF₃ has been proposed to be a new coating material to improve electrochemical properties of pristine materials. The AlF₃-coated LiCoO₂,^{17,18} LiNi_{0.8}Co_{0.1}Mn_{0.1}O₂,¹⁹ LiNi_{1/3}Co_{1/3}Mn_{1/3}O₂^{20,21} all showed enhanced electrochemical performance as compared to the related pristine materials. The detailed mechanism of surface coating on the electrochemical performance of the materials still needs further investigation.

Differential electrochemical mass spectrometry (DEMS) technique, as an effective in situ tool, has been developed to detect the gaseous reaction products that are evolved during solid-electrolyte interface (SEI) formation and/or electrode reaction.^{22,23} With DEMS, the intensity change of *m/z* signals can be detected as a function of time and/or potential. At the same time, these signals can be correlated with current peaks in cyclic voltammogram or plateaus on galvanostatic charge/discharge profiles. It has also been used to demonstrate the mechanism of oxygen loss during the initial charge process in Li[Ni_{0.2}Li_{0.2}Mn_{0.6}]O₂²⁴ for lithium-ion battery.

Here, we have studied the effects of AlF₃ coating on the structure, thermal stability, interfacial impedance, initial irreversible capacity loss, and electrochemical performance of Li[Li_{0.2}Mn_{0.54}Ni_{0.13}Co_{0.13}]O₂. Meanwhile, we also adopt an in situ DEMS technique to investigate the influence of AlF₃ coating on the gaseous reaction products of O₂ and CO₂ during potential scan and propose a mechanism for explaining our results.

Experimental

The precursor of the Li[Li_{0.2}Mn_{0.54}Ni_{0.13}Co_{0.13}]O₂ compound such as M(OH)₂ (M = Ni, Mn, Co) was synthesized by a coprecipitation method.²⁵ Then the M(OH)₂ and stoichiometric amount of LiOH·H₂O were pressed into pellets and precalcined at 480°C for 10 h, then ground and made into new pellets. The target compound was finally gained by quenching the new pellets after being fired at 900°C for 3 h.²⁶ The procedure of preparing the AlF₃-coated Li[Li_{0.2}Mn_{0.54}Ni_{0.13}Co_{0.13}]O₂ is described in detail in Ref. 21. To prepare AlF₃-coated material, ammonium fluoride (Aldrich) and aluminum nitrate dehydrate were separately dissolved in distilled water. After Li[Li_{0.2}Mn_{0.54}Ni_{0.13}Co_{0.13}]O₂ powders were dispersed into the aluminum nitrate solution, the NH₄F solution was slowly added to the solution. The amount of AlF₃ was 2.5 mol % of the Li[Li_{0.2}Mn_{0.54}Ni_{0.13}Co_{0.13}]O₂ powders. The above-presented solution was constantly stirred at 80°C for 5 h, followed by a slow evaporation of solvent. The obtained coated precursor was heated at 400°C for 5 h under the flow of nitrogen gas.

X-ray diffraction (XRD) of these samples was performed on a Panalytical X'Pert diffractometer (Holland) with Cu K α radiation operated at 40 kV and 30 mA. Data were collected in 2 θ range of 10–90° at 4°/min. The lattice parameters were refined by the Rietveld method with General Structure Analysis Software (GSAS program, Los Alamos National Laboratory, USA). Scanning electron microscopy (SEM) was performed on LEO1530 (Oxford Company). The thermal stability of the Li[Li_{0.2}Mn_{0.54}Ni_{0.13}Co_{0.13}]O₂ electrodes at a delithiated state of 4.8 V was examined, by means of differential scanning calorimetry (DSC) with a Netzsch STA 409PC thermal analysis system (Netzsch, Germany) from 50 to 350°C at a heating rate of 5°C/min.

Electrochemical measurements were carried out using R2025 coin-type cells. The positive electrodes were prepared by coating a mixture containing 80% active materials, 10% acetylene black, 10% poly(vinylidene fluoride) binder on circular Al current collector foils

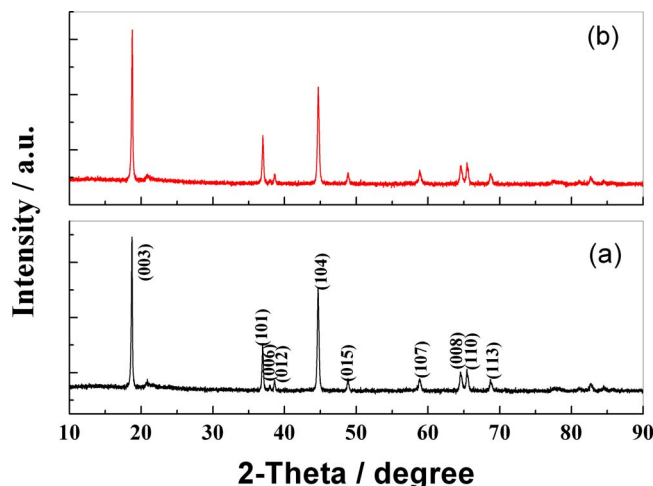


Figure 1. (Color online) XRD patterns of the pristine and AlF₃-coated Li[Li_{0.2}Mn_{0.54}Ni_{0.13}Co_{0.13}]O₂.

with diameter of 1.6 cm, followed by drying at 120°C for 1 h. The electrode weight was controlled between 5 and 6 mg, with thickness of about 20 μ m. Electrochemical cells were assembled with the positive electrodes as-prepared, metallic lithium foil as counter electrode, Cellgard 2300 as separator, and 1 M LiPF₆ dissolved in ethyl carbonate (EC) and dimethyl carbonate (DMC) (1:1 in volume) as electrolyte in an argon-filled glove box (Labmaster100, Mbraun, Germany). Charge–discharge experiments were performed galvanostatically with current density of 18 and 90 mA/g between 2.0 and 4.8 V on battery testers (Land CT2001A). Capacities were calculated by only considering the active mass of the electrodes. All the potentials throughout the paper are in reference to the Li/Li⁺ couple. The cells were cycled at room temperature and 50°C to compare cyclic performances of the pristine and AlF₃-coated samples. Electrochemical impedance spectroscopy (EIS) of the cells was measured at charged state of 4.3 V at frequencies from 0.01 to 100,000 Hz with perturbation amplitude of 10 mV using a potentio/galvanostat PGSTAT 30 frequency response analyzer (Eco Chemie, The Netherlands).

In situ DEMS measurements were carried out to detect the O₂ and CO₂ gases generated during the potential scanning process. The measurements were performed using a quadrupole mass spectrometer (Aeolos QMS 403 C, Netzsch, Germany) and an electrochemical cell, which has been described in detail in a previous paper.²⁷ In brief, the cell body was made of polytetrafluoroethylene, and an O-ring was used to seal the cell. A nonwettability of porous membrane was added as a solvent barrier between the cell and the vacuum system of the mass spectrometer. The positive electrodes were prepared by the same method as mentioned earlier for electrochemical measurements. The counter electrode was made by pressing metallic lithium on a copper current collector. The cell potential was scanned from open circuit potential to 4.8 V with a scan rate of 0.2 mV/s and then held at 4.8 V for 2 h. During the measurements, a constant stream of argon (40 mL/s) was flowed through the head space of the cell. O₂ and CO₂ gas evolved as the electrode rose within the electrolyte to the head space and was pumped off, together with the argon carrier gas, to the mass spectrometer. The mass signals were recorded simultaneously as a function of cell voltage and time. The measurements were carried out at room temperature (25°C).

Results and Discussion

XRD structural characterization.—Figure 1 shows the X-ray diffraction XRD patterns and Miller indices of the pristine and AlF₃-coated Li[Li_{0.2}Mn_{0.54}Ni_{0.13}Co_{0.13}]O₂ samples. Except for the

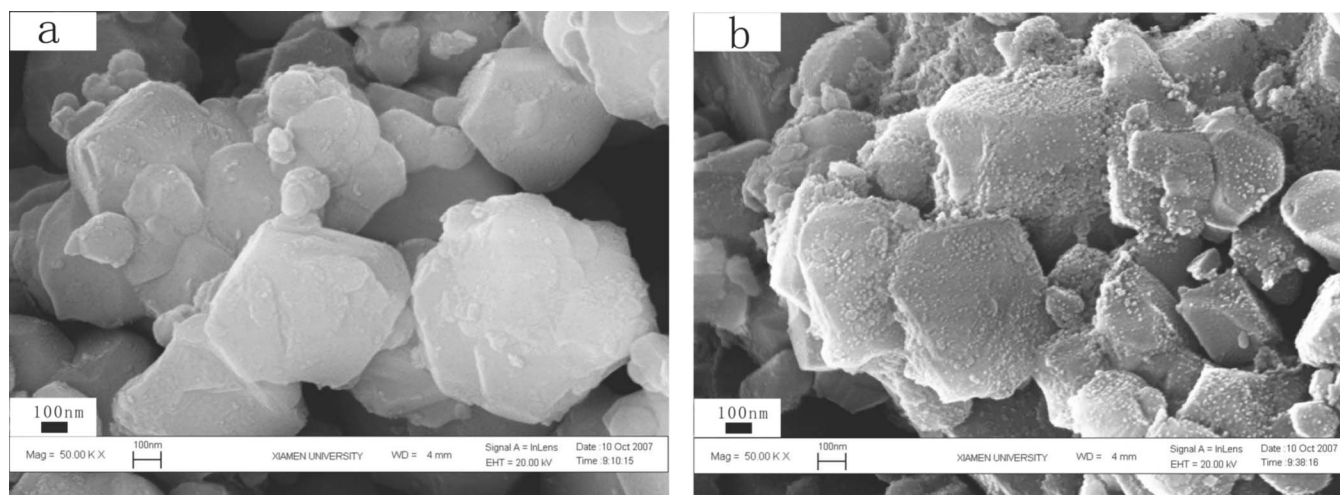


Figure 2. SEM images of the (a) pristine and (b) AlF_3 -coated $\text{Li}[\text{Li}_{0.2}\text{Mn}_{0.54}\text{Ni}_{0.13}\text{Co}_{0.13}]\text{O}_2$.

superlattice peaks between 20 and 25°, all peaks of the XRD patterns could be indexed as an O3-type structure. The weak peaks between 20 and 25°, which cannot be indexed to R-3m symmetry, are consistent with the LiMn_6 cation arrangement that occurs in the transition metal layers of Li_2MnO_3 regions or nanodomains, which can be indexed to the monoclinic unit cell C2/m.^{28,29} As compared to the conventional layered material, e.g., LiCoO_2 or LiNiO_2 , $\text{Li}[\text{Li}_{0.2}\text{Mn}_{0.54}\text{Ni}_{0.13}\text{Co}_{0.13}]\text{O}_2$ is more complicated in structure for up to four cations sharing a single site. This suggests that additional information is badly needed to determine the individual element. For example, a careful synchrotron study should be conducted as reported by Whitfield et al.³⁰ The combined neutron and resonant diffraction study for a similar electrode material, $\text{Li}_{1.2}\text{Mn}_{0.4}\text{Ni}_{0.3}\text{Co}_{0.1}\text{O}_2$, clearly showed that the cations in the transition metal layers were not homogeneously distributed and that the Li and Mn cations, in particular, occupy predominantly the crystallographic sites as they do in Li_2MnO_3 . Because of the paucity of data, lattice parameters were refined using the high-symmetry trigonal space group, R-3m, rather than the low-symmetry monoclinic space group, C2/m. Lattice parameters a and c calculated by the Rietveld refinement are $a = 2.8535 \text{ \AA}$ and $c = 14.2372 \text{ \AA}$ for pristine $\text{Li}[\text{Li}_{0.2}\text{Mn}_{0.54}\text{Ni}_{0.13}\text{Co}_{0.13}]\text{O}_2$ and $a = 2.8543 \text{ \AA}$ and $c = 14.2371 \text{ \AA}$ for the AlF_3 -coated material. In comparison with the pristine $\text{Li}[\text{Li}_{0.2}\text{Mn}_{0.54}\text{Ni}_{0.13}\text{Co}_{0.13}]\text{O}_2$, lattice parameters a and c of the coated material show no obvious changes. No extra reflection peaks corresponding to the Al-related impurity phases are seen for the AlF_3 -coated sample, which is probably due to a small quantity and/or amorphous nature of AlF_3 .

SEM images.— SEM images of the surface morphology of the pristine and AlF_3 -coated materials are given in Fig. 2. It can be seen that $\text{Li}[\text{Li}_{0.2}\text{Mn}_{0.54}\text{Ni}_{0.13}\text{Co}_{0.13}]\text{O}_2$ powders prepared by coprecipitation method are not very uniform in particle size. However, the surface of the pristine $\text{Li}[\text{Li}_{0.2}\text{Mn}_{0.54}\text{Ni}_{0.13}\text{Co}_{0.13}]\text{O}_2$ powders is somewhat smooth. In contrast, the surface of $\text{Li}[\text{Li}_{0.2}\text{Mn}_{0.54}\text{Ni}_{0.13}\text{Co}_{0.13}]\text{O}_2$ powders becomes considerably rough after coating. It could be distinguished that the AlF_3 coating layer is composed of a large number of nanosized AlF_3 particles, which distribute independently or connect to each other. Although the AlF_3 particles do not coat the $\text{Li}[\text{Li}_{0.2}\text{Mn}_{0.54}\text{Ni}_{0.13}\text{Co}_{0.13}]\text{O}_2$ powders completely, to our knowledge, a large amount of nanosized AlF_3 particles attaching tightly on the surface of the parent compound would greatly reduce the surface area exposed to the electrolyte during charge/discharge cycling.

Electrochemical performance.— Figure 3 compares the initial charge/discharge profiles of pristine and AlF_3 -coated

$\text{Li}[\text{Li}_{0.2}\text{Mn}_{0.54}\text{Ni}_{0.13}\text{Co}_{0.13}]\text{O}_2$ materials in the voltage range of 2.0–4.8 V at 0.1 C rate. It is clearly shown that the first charge profiles are both accompanied with irreversible voltage plateaus for oxidation beyond the formal oxidation potential of Ni^{2+} to Ni^{4+} , and Co^{3+} to Co^{4+} . The voltage plateaus have been assigned to an irreversible loss of oxygen from the lattice based on DEMS results²⁴ and in situ XRD studies.³¹ The theoretical capacity, based on complete extraction of lithium (1.2 Li per $\text{Li}[\text{Li}_{0.2}\text{Mn}_{0.54}\text{Ni}_{0.13}\text{Co}_{0.13}]\text{O}_2$ formula unit), is 377 mA h/g. The theoretical discharge capacity, based on the mass of the discharged rock-salt product after the first charge/discharge cycle, $0.5 \text{ LiMnO}_2 \cdot 0.5 \text{ LiNi}_{1/3}\text{Co}_{1/3}\text{Mn}_{1/3}\text{O}_2$, is 283 mA h/g, which is higher than the theoretical capacity of standard LiCoO_2 electrode (274 mA h/g). However, the actual charge capacity of the pristine and AlF_3 -coated $\text{Li}[\text{Li}_{0.2}\text{Mn}_{0.54}\text{Ni}_{0.13}\text{Co}_{0.13}]\text{O}_2$ is only 324.5 and 314.0 mA h/g, respectively. Besides the large kinetic barrier, this capacity disparity possibly results from the residual Li_2MnO_3 component, which is electrochemically inactive, remaining in the bulk electrode. The residual inactive Li_2MnO_3 may serve to stabilize the electrochemically active LiMO_2 and the partially activated Li_2MnO_3 during cycling process.¹⁴

Compared to the charge–discharge curves of the pristine $\text{Li}[\text{Li}_{0.2}\text{Mn}_{0.54}\text{Ni}_{0.13}\text{Co}_{0.13}]\text{O}_2$, the charging potential curve for the

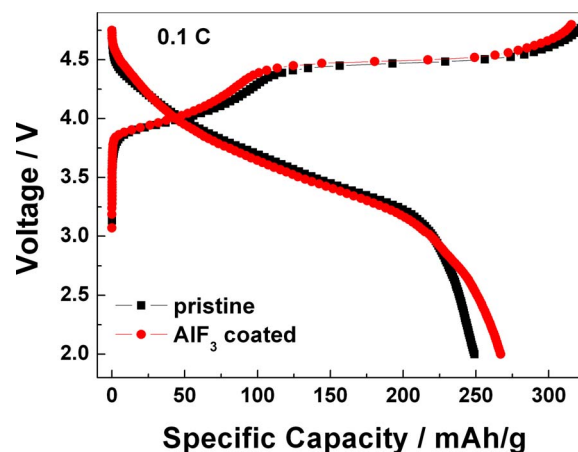


Figure 3. (Color online) The first charge/discharge profiles of the pristine and AlF_3 -coated $\text{Li}[\text{Li}_{0.2}\text{Mn}_{0.54}\text{Ni}_{0.13}\text{Co}_{0.13}]\text{O}_2$ over the voltage range of 2.0–4.8 V at 0.1 C rate.

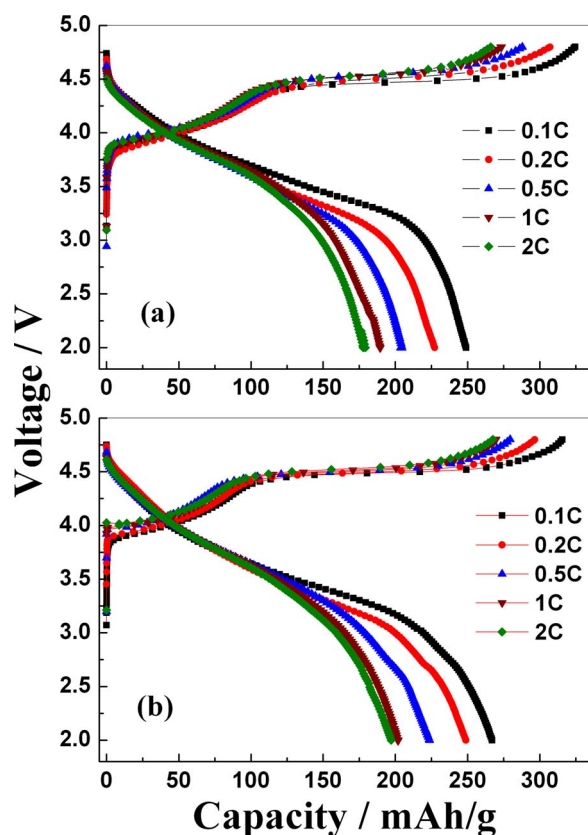


Figure 4. (Color online) The first charge/discharge profiles of the (a) pristine and (b) AlF_3 -coated $\text{Li}[\text{Li}_{0.2}\text{Mn}_{0.54}\text{Ni}_{0.13}\text{Co}_{0.13}]\text{O}_2$ at different current density (1 C = 180 mA/g).

AlF_3 -coated material is a little higher whereas the discharge potential curve is slightly lower, indicating that a resistive coating layer exists on the surface of AlF_3 -coated $\text{Li}[\text{Li}_{0.2}\text{Mn}_{0.54}\text{Ni}_{0.13}\text{Co}_{0.13}]\text{O}_2$ powders. This phenomenon is also consistent with the result reported for AlF_3 -coated $\text{LiNi}_{1/3}\text{Co}_{1/3}\text{Mn}_{1/3}\text{O}_2$.²⁰ By comparison, it also can be found that, after surface modification with AlF_3 , the charge capacity decreases from 324.5 to 314.0 mA h/g, while the discharge capacity increases from 249.0 to 267.0 mA h/g, which means that the irreversible capacity loss (ICL) decreases from 75.5 to 47 mA h/g. As it was reported,¹⁰ we are also convinced that the higher discharge capacity and the lower ICL of AlF_3 -coated material are attributable to a suppression of the reaction between the electrolyte and active material at high potential and an optimization of the SEI layer. Meanwhile, the result also signifies that the initial coulombic efficiency is enhanced by AlF_3 coating, increasing from 76.7% for pristine material to 85.0% for AlF_3 -coated material.

The rate capability is an important factor for battery performance because the charge time of batteries in portable electric devices depends on the rate of Li^+ extraction from and insertion into the positive electrode. The rate capabilities of the pristine and AlF_3 -coated $\text{Li}[\text{Li}_{0.2}\text{Mn}_{0.54}\text{Ni}_{0.13}\text{Co}_{0.13}]\text{O}_2$ investigated in the voltage range of 2.0–4.8 V are shown in Fig. 4a and b, respectively. When the charge/discharge rate increases from 0.1 to 2 C, the discharge capacity of the pristine $\text{Li}[\text{Li}_{0.2}\text{Mn}_{0.54}\text{Ni}_{0.13}\text{Co}_{0.13}]\text{O}_2$ decreases to 177.9 mA h/g, which is only 71.4% capacity retention vs the capacity of 0.1 C (249 mA h/g). In contrast, the AlF_3 -coated material shows 73.8% (from 267 to 197 mA h/g) capacity retention. Therefore, the rate capability of the $\text{Li}[\text{Li}_{0.2}\text{Mn}_{0.54}\text{Ni}_{0.13}\text{Co}_{0.13}]\text{O}_2$ is somewhat improved by AlF_3 coating.

Figure 5 displays the cyclic performances of pristine and AlF_3 -coated $\text{Li}[\text{Li}_{0.2}\text{Mn}_{0.54}\text{Ni}_{0.13}\text{Co}_{0.13}]\text{O}_2$ cycled at 0.2 and 0.5 C

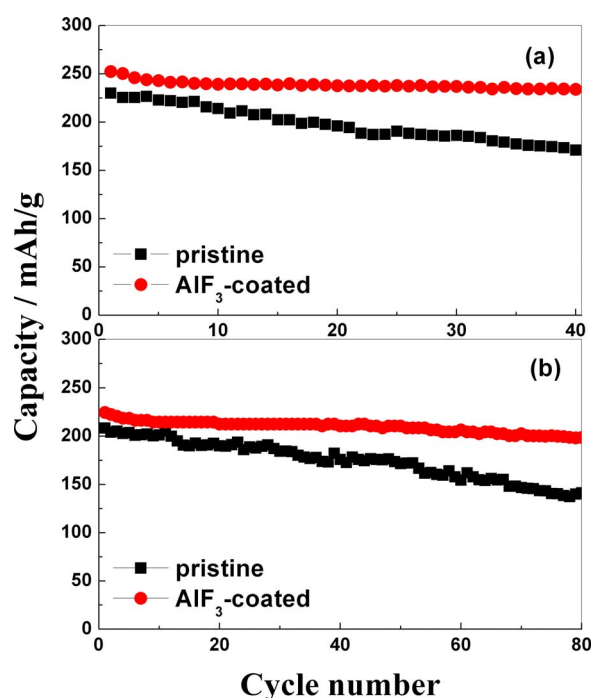


Figure 5. (Color online) Cycle-life performance of the pristine and AlF_3 -coated $\text{Li}[\text{Li}_{0.2}\text{Mn}_{0.54}\text{Ni}_{0.13}\text{Co}_{0.13}]\text{O}_2$ electrodes at room temperature, over the voltage range of 2.0–4.8 V.

rate at room temperature, respectively. It is obviously shown that the cyclic performance is significantly improved by AlF_3 coating. After being charged/discharged at 0.2 C rate for 40 cycles, the AlF_3 -coated $\text{Li}[\text{Li}_{0.2}\text{Mn}_{0.54}\text{Ni}_{0.13}\text{Co}_{0.13}]\text{O}_2$ presents a better capacity retention of 92.7% (vs to the first discharge capacity), while the pristine material shows only capacity retention of 74.4%. Similar improvement is also observed when the cells cycled at 0.5 C rate. Compared to capacity retention of 67.8% after 80 cycles for pristine sample, the AlF_3 -coated sample shows higher capacity retention of 87.9%.

Figure 6 describes the cyclic performance and capacity retentions of the pristine and AlF_3 -coated $\text{Li}[\text{Li}_{0.2}\text{Mn}_{0.54}\text{Ni}_{0.13}\text{Co}_{0.13}]\text{O}_2$ materials at 0.5 C under elevated temperature of 50°C for 80 cycles. On one hand, the AlF_3 -coated $\text{Li}[\text{Li}_{0.2}\text{Mn}_{0.54}\text{Ni}_{0.13}\text{Co}_{0.13}]\text{O}_2$ exhibits higher initial discharge capacity (248 mA h/g) than that of pristine $\text{Li}[\text{Li}_{0.2}\text{Mn}_{0.54}\text{Ni}_{0.13}\text{Co}_{0.13}]\text{O}_2$ (236 mA h/g). Moreover, the AlF_3 -coated $\text{Li}[\text{Li}_{0.2}\text{Mn}_{0.54}\text{Ni}_{0.13}\text{Co}_{0.13}]\text{O}_2$ shows only 17.4% of capacity loss after 80 cycles, while the pristine material shows 28.8% capacity loss. This suggests that high temperature performance of the material is also evidently improved by AlF_3 coating.

DSC.—The thermal stability of the positive electrode materials at delithiated state is of great importance related to battery safety. The thermal stability of the pristine and AlF_3 -coated $\text{Li}[\text{Li}_{0.2}\text{Mn}_{0.54}\text{Ni}_{0.13}\text{Co}_{0.13}]\text{O}_2$ electrodes were measured by DSC. Figure 7 provides the DSC profiles of the pristine and AlF_3 -coated electrodes charged to 4.8 V. Not only is the onset temperature of thermal decomposition increased by AlF_3 coating, i.e., from 206.6 to 223.8°C, but also the heat associated with the exothermic peak is greatly reduced. The AlF_3 -coated electrode produces heat of only 538.0 J/g, compared to 924.5 J/g for pristine electrode. This result suggests that coating $\text{Li}[\text{Li}_{0.2}\text{Mn}_{0.54}\text{Ni}_{0.13}\text{Co}_{0.13}]\text{O}_2$ with AlF_3 retards the reaction between electrolyte and electrode material significantly.

Electrochemical impedance spectra analysis.—EIS has been performed to understand the improved electrochemical performance

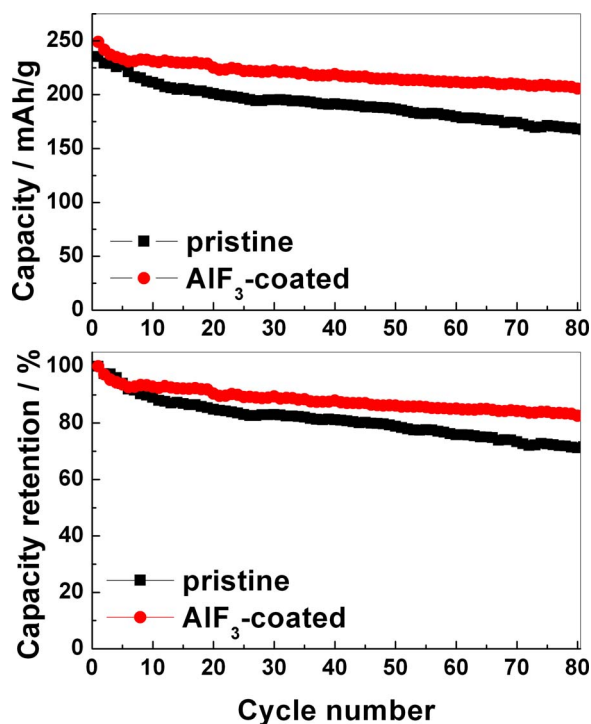


Figure 6. (Color online) Cycle-life performance of the pristine and AlF₃-coated Li[Li_{0.2}Mn_{0.54}Ni_{0.13}Co_{0.13}]O₂ electrodes at 0.5 C under elevated temperature (50°C), over the potential range 2.0–4.8 V.

of AlF₃-coated Li[Li_{0.2}Mn_{0.54}Ni_{0.13}Co_{0.13}]O₂. The measurements were carried out in the charged state to 4.3 V at the 2nd, 10th, 20th, 30th, and 40th cycles. The measured impedance spectra are presented in Fig. 8a and b and the results fitted with the equivalent circuit inset in Fig. 9. Similar studies were also reported for many positive electrode materials, such as TiO₂-coated LiNi_{0.8}Co_{0.2}O₂,^{32,33} and Al₂O₃-coated LiNi_{1/3}Co_{1/3}Mn_{1/3}O₂.³⁴ Similarly, a high-frequency semicircle, an intermediate-frequency semicircle, and low-frequency tails are observed. Generally, the high-frequency semicircle is related to the passivating surface film, the SEI. The intermediate-frequency semicircle is ascribed to the charge transfer process resistance in the electrode/electrolyte interface. The low-frequency tail is associated with the Li⁺ ion diffusion process in the positive electrode.

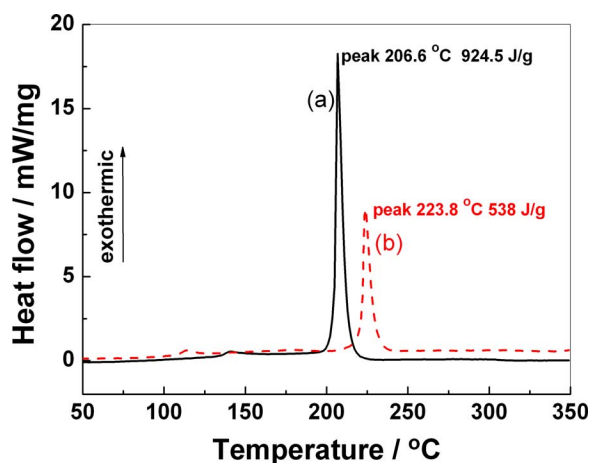


Figure 7. (Color online) DSC profiles of the pristine and AlF₃-coated Li[Li_{0.2}Mn_{0.54}Ni_{0.13}Co_{0.13}]O₂ electrodes at charged state to 4.8 V.

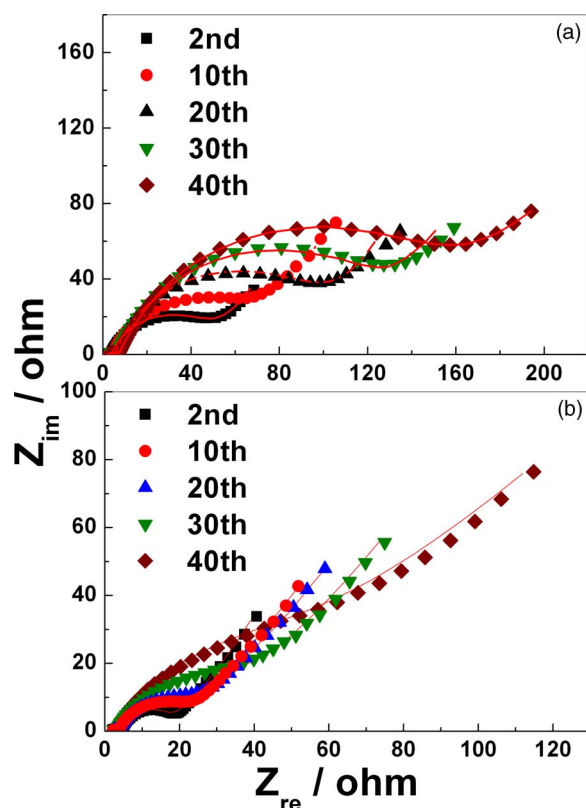


Figure 8. (Color online) Nyquist plots of the (a) Li/pristine Li[Li_{0.2}Mn_{0.54}Ni_{0.13}Co_{0.13}]O₂ and (b) the Li/AlF₃-coated Li[Li_{0.2}Mn_{0.54}Ni_{0.13}Co_{0.13}]O₂ at 0.5 C rate.

Figure 9 presents the variation of R_{ct} values for the pristine and AlF₃-coated Li[Li_{0.2}Mn_{0.54}Ni_{0.13}Co_{0.13}]O₂ electrodes. The results show that the R_{ct} value of the pristine electrode increases faster than the AlF₃-coated material. The R_{ct} value of the pristine material is 39.4 Ω in the second cycle, increasing rapidly with cycling, and reaches up to 143.1 Ω after 40 cycles. It is anticipated that the SEI, formed from reaction between electrode and electrolyte, acts as a barrier between active material and the electrolyte, and thus it would increase R_{ct} value. In contrast, AlF₃-coated electrode shows smaller

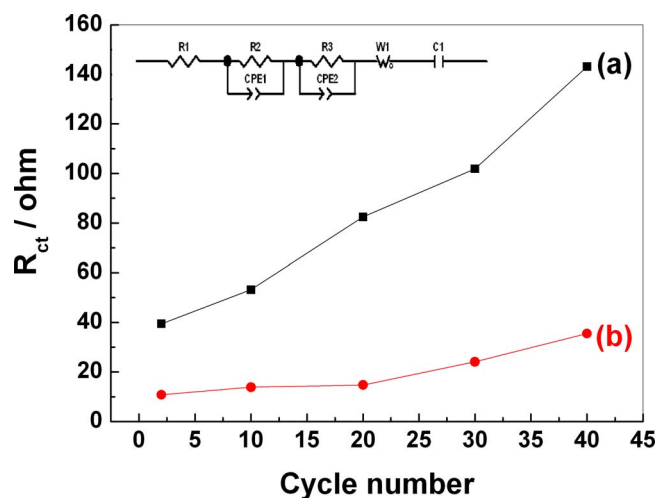


Figure 9. (Color online) R_{ct} values as a function of cycle number for the pristine and AlF₃-coated Li[Li_{0.2}Mn_{0.54}Ni_{0.13}Co_{0.13}]O₂ electrodes. The inset is the equivalent circuit used to fit the measured spectra.

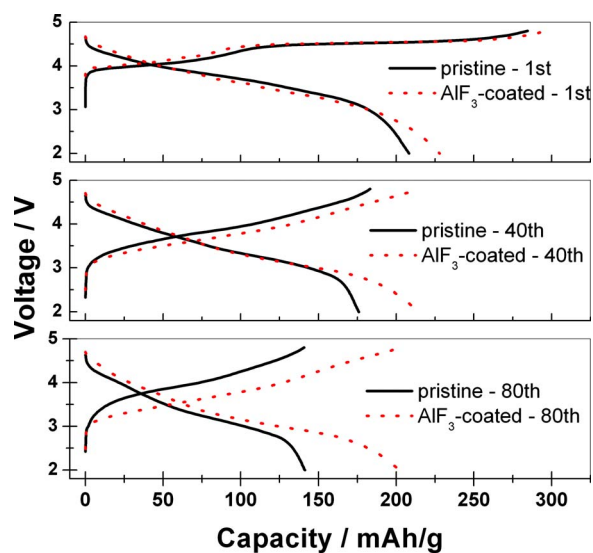


Figure 10. (Color online) Charge/discharge profiles of the 1st, 40th, and 80th cycles for pristine and AlF_3 -coated electrodes.

R_{ct} values than the uncoated electrode and slow increase of charge-transfer impedance. The R_{ct} value of AlF_3 -coated electrode exhibits 10.7Ω after one cycle, increasing slowly, and reaches only 35.5Ω at the 40th cycle, which is still smaller than that of the pristine material in the 2nd cycle.

Recently, Sun et al.¹⁷ reported that the excellent capacity retention of AlF_3 -coated LiCoO_2 at the cutoff voltage of 4.5 V originated from the lower R_{ct} and reduced cobalt dissolution. Sun et al.²⁰ also reported that the enhanced electrochemical performance of AlF_3 -coated $\text{LiNi}_{1/3}\text{Co}_{1/3}\text{Mn}_{1/3}\text{O}_2$ originated from the lower and stable charge transfer resistance and from the stabilized host structure of $\text{LiNi}_{1/3}\text{Co}_{1/3}\text{Mn}_{1/3}\text{O}_2$. In this respect, it could be concluded that the AlF_3 coating layer has prevented electrode/electrolyte interfacial degradation, which is caused by a very complicated process as a result of decomposition of the electrolyte at high potential and from the attack of acidic species in the electrolyte. Consequently, AlF_3 coating, with stable electrode/electrolyte interface, can significantly prohibit the increase of charge transfer resistance, which in turn limits the increase of the total cell resistance and enhances the electrochemical performance of AlF_3 -coated $\text{Li}[\text{Li}_{0.2}\text{Mn}_{0.54}\text{Ni}_{0.13}\text{Co}_{0.13}]\text{O}_2$.

Figure 10 compares the voltage/capacity curves of the pristine and AlF_3 -coated $\text{Li}[\text{Li}_{0.2}\text{Mn}_{0.54}\text{Ni}_{0.13}\text{Co}_{0.13}]\text{O}_2$ in the 1st, 40th, and 80th cycles at 90 mA/g at room temperature. It is observed that the polarization of AlF_3 -coated electrodes in the first cycle is larger than that of the uncoated sample, and a little difference between charge and discharge curves in comparison with that of the pristine electrodes. However, the polarization of pristine electrode increases more dramatically during cycling and becomes significantly higher than that of AlF_3 -coated electrode after 80 cycles. These results are also consistent with those of the EIS experiments.

DEMS.—To date, a number of authors have proposed the mechanisms for improved electrochemical performance derived from surface coating. Chen and Dahn reported that the excellent capacity retention of LiCoO_2 coated with ZrO_2 , Al_2O_3 , and SiO_2 charged to 4.5 V was due to the suppression of side reaction between positive electrode and electrolyte, which significantly reduced the high impedance layer on the surface of LiCoO_2 during electrochemical cycling.^{35,36} Sun et al.^{37,38} clarified that the excellent cyclability of the ZnO-coated $\text{LiNi}_{0.5}\text{Mn}_{1.5}\text{O}_4$ electrode was ascribed to significantly reduced HF content in the electrolyte, which in turn resulted in the suppression of Mn dissolution. The ZnO in these cells acted as a HF getter in the electrolyte. To further understand the

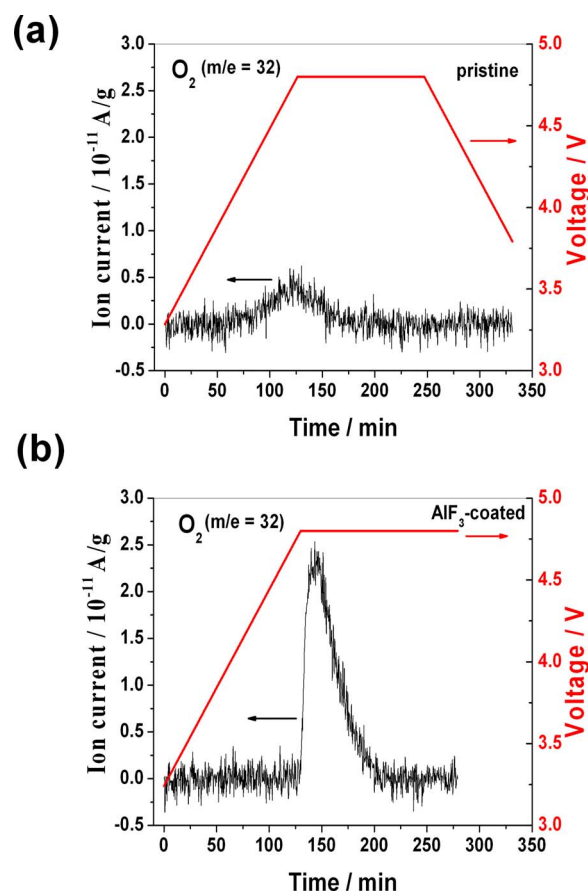


Figure 11. (Color online) DEMS measurements of the O_2 evolution on $\text{Li}[\text{Li}_{0.2}\text{Mn}_{0.54}\text{Ni}_{0.13}\text{Co}_{0.13}]\text{O}_2$ electrodes. (a) Pristine and (b) AlF_3 -coated sample.

improved performance of AlF_3 -coated material, DEMS was adopted to detect gaseous reaction products which evolved during potential scan. The results of gaseous reaction products, in particular, O_2 and CO_2 , are shown in Fig. 11 and 12.

Similar to that oxygen loss of $\text{Li}[\text{Ni}_{0.2}\text{Li}_{0.2}\text{Mn}_{0.6}]\text{O}_2$ during charge process,²⁴ oxygen evolutions were observed for both the pristine and AlF_3 -coated $\text{Li}[\text{Li}_{0.2}\text{Mn}_{0.54}\text{Ni}_{0.13}\text{Co}_{0.13}]\text{O}_2$ electrodes during potential scan. For pristine electrode, surprisingly, O_2 evolution starts at a voltage of 4.30 V with a maximum at 4.78 V. For coated electrode, O_2 evolution starts at a higher voltage of 4.75 V and reaches its maximum at the potentiostatic stage. It may be inconvinient to attribute this potential difference to the polarization from AlF_3 coating layer. In addition, the shapes of signal curves are quite different. It is speculated that a little of the lattice oxygen at the electrode surface turned active and began to lose when Ni^{2+} and Co^{3+} were oxidized to Ni^{4+} and Co^{4+} . Here, we cannot exclude the possibility that Li^+ in the electrode exchanges with H^+ generated by oxidation of the alkyl carbonate electrolyte at ca. 4.5 V. However, considering that our DEMS experiments were carried out at room temperature and based on the results reported in Ref. 12, we are convinced that Li^+ is removed dominantly accompanied by oxygen loss beyond the oxidation of $\text{Ni}^{2+}\text{--Ni}^{4+}$ and $\text{Co}^{3+}\text{--Co}^{4+}$ in this potential region.

Different from the conventional layered structural material, without extra lithium in the transition metal (TM) layer, the main origins of CO_2 evolution during the charging process for the so-called lithium-rich $\text{Li}[\text{Li}_{0.2}\text{Mn}_{0.54}\text{Ni}_{0.13}\text{Co}_{0.13}]\text{O}_2$ are as follows: (i) from the oxidation of the electrolyte by the oxidative TM ions, Ni^{4+} and Co^{4+} . The related mechanisms of oxidation of EC and DMC have been reported previously.³⁹ (ii) From the partial oxidation of the

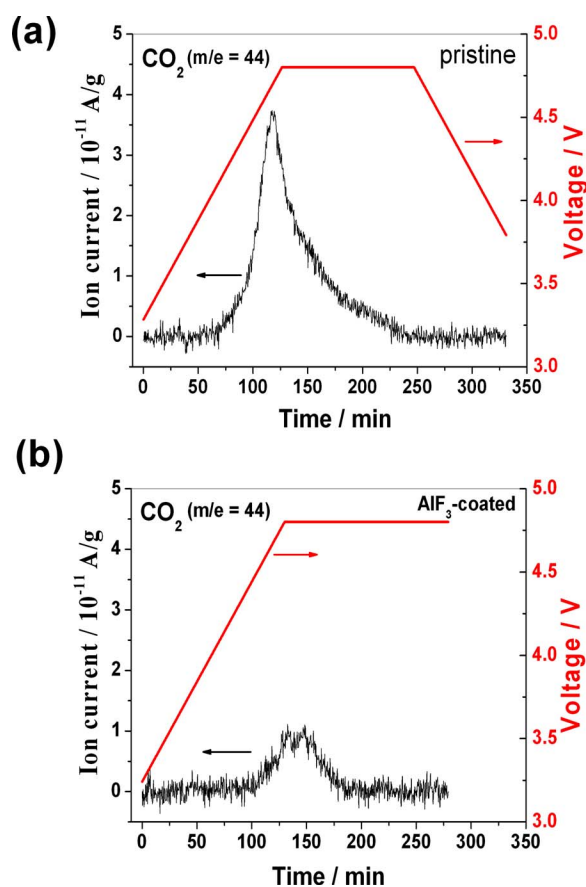


Figure 12. (Color online) DEMS measurements of the CO_2 evolution on $\text{Li}[\text{Li}_{0.2}\text{Mn}_{0.54}\text{Ni}_{0.13}\text{Co}_{0.13}]\text{O}_2$ electrodes. (a) Pristine and (b) AlF_3 -coated sample.

electrolyte by the evolved oxygen.²³ In detail, for the pristine one, the signal of CO_2 evolution appears at 4.10 V, and reaches a maximum at 4.70 V, while for the AlF_3 -coated one, the CO_2 evolution signal turns up at a higher potential of 4.45 V and reaches its maximum at the beginning of the potentiostatic stage. This suggests that the evolution of CO_2 is greatly delayed by AlF_3 coating.

In comparison, it is evidently shown that the signal of detected O_2 for the pristine electrode is weaker than that of AlF_3 -coated one. The amount of detected O_2 for the pristine electrode, calculated from integration of the signal, is estimated to be only 1/4 of the AlF_3 -coated one. However, the signal of CO_2 gas evolution for the pristine electrode is considerably stronger than that for the AlF_3 -coated one by a factor of 5. This means that amount of CO_2 is not proportional to that of O_2 , suggesting that the CO_2 is not from the oxidation of electrolyte by O_2 molecules. It is proposed that the oxygen is extracted out with high activity from the structural lattice to the electrode's surface in terms of oxygen atoms which combine to form O_2 molecules subsequently. For pristine material, the active oxygen atoms oxidize the electrolyte directly, leading to the evident evolution of CO_2 . In contrast, for AlF_3 -coated material, the activity of the extracted oxygen atoms decreases while the oxygen atoms pass through the coating layer. Most oxygen atoms with reduced activity combine to form stable oxygen molecules before they contact with electrolyte, which results in less oxidation of the electrolyte. Therefore, the pristine electrode exhibits a smaller amount of O_2 and a larger amount of CO_2 , compared to AlF_3 -coated material.

From this point of view, it suggests that AlF_3 coating does provide a buffer layer to mitigate the activity of the evolved oxygen, which greatly suppresses the decomposition of the electrolyte. The decreased decomposition of electrolyte will keep the electrolyte

more stable during cycling. Although only results of first cycle have been obtained, it can be expected that the electrolyte will be more enduring for extended cycling after AlF_3 coating, which is one of the crucial reasons accounting for the improved electrochemical performance of the coated materials. In addition, it has also been found that the amount of gaseous product of CO_2 decreased significantly in the following cycles. The detailed work and further research on the electrolyte decomposition mechanism is still ongoing in our lab.

Conclusion

The $\text{Li}[\text{Li}_{0.2}\text{Mn}_{0.54}\text{Ni}_{0.13}\text{Co}_{0.13}]\text{O}_2$ samples coated with AlF_3 have been prepared and investigated. The AlF_3 -coated $\text{Li}[\text{Li}_{0.2}\text{Mn}_{0.54}\text{Ni}_{0.13}\text{Co}_{0.13}]\text{O}_2$ exhibited superior electrochemical performance in comparison with the pristine material, including high initial discharge capacity of 267 mA h/g, low initial irreversible capacity loss, better cyclic performance, and higher rate capability. Meanwhile, the thermal stability of the materials was also improved significantly after AlF_3 coating. The improved electrochemical performance could be attributed to the "buffer" layer provided by AlF_3 coating, through which oxygen atoms with high activity generated at high potential combined to form O_2 molecules with low activity. Consequently, it results in the reduction of the activity of the evolved oxygen species and suppression of the decomposition of electrolyte. This effect has resulted in less oxidation of electrolyte components, prevented the electrode/electrolyte interfacial degradation, and thus suppressed the increase of charge transfer resistance.

Acknowledgments

This work was financially supported by the National Basic Research Program of China (973 Program) (grant no. 2007CB209702), and National Natural Science Foundation of China (NNSFC, grant no. 20433060, grant no. 20473068, and grant no. 29925310).

Xiamen University assisted in meeting the publication costs of this article.

References

1. T. Ohzuku and R. Brodd, *J. Power Sources*, **174**, 449 (2007).
2. T. Ohzuku and Y. Makimura, *Chem. Lett.*, **8**, 744 (2001).
3. N. Yabuuchi and T. Ohzuku, *J. Power Sources*, **119**, 171 (2003).
4. M. M. Thackeray, *Prog. Solid State Chem.*, **25**, 1 (1997).
5. T. Ohzuku, K. Ariyoshi, Y. Makimura, N. Yabuuchi, and K. Sawai, *Electrochemistry (Tokyo, Jpn.)*, **73**, 2 (2005).
6. C. S. Johnson, J.-S. Kim, C. Lefief, N. Li, J. T. Vaughey, and M. M. Thackeray, *Electrochem. Commun.*, **6**, 1085 (2004).
7. M. M. Thackeray, C. S. Johnson, J. T. Vaughey, N. Li, and S. A. Hackney, *J. Mater. Chem.*, **15**, 2257 (2005).
8. C. S. Johnson, N. Li, C. Lefief, and M. M. Thackeray, *Electrochem. Commun.*, **9**, 787 (2007).
9. M. M. Thackeray, S. H. Kang, C. S. Johnson, J. T. Vaughey, R. Benedek, and S. A. Hackney, *J. Mater. Chem.*, **17**, 3112 (2007).
10. Y. Wu and A. Manthiram, *Electrochem. Solid-State Lett.*, **9**, A221 (2006).
11. A. Du Pasquier, A. Blyr, P. Courjal, D. Larcher, G. Amatucci, B. Gérard, and J. M. Tarascon, *J. Electrochem. Soc.*, **146**, 428 (1999).
12. A. D. Robertson and P. G. Bruce, *Chem. Mater.*, **15**, 1984 (2003).
13. S. H. Kang and K. Amine, *J. Power Sources*, **146**, 654 (2005).
14. S. H. Kang and M. M. Thackeray, *J. Electrochem. Soc.*, **155**, A269 (2008).
15. Y.-J. Kang, J. H. Kim, S. W. Lee, and Y. K. Sun, *Electrochim. Acta*, **50**, 4784 (2005).
16. S. T. Myung, K. Izumi, S. Komaba, Y. K. Sun, H. Yashiro, and N. Kumagai, *Chem. Mater.*, **17**, 3695 (2005).
17. Y. K. Sun, J. M. Han, S. T. Myung, S. W. Lee, and K. Amine, *Electrochem. Commun.*, **8**, 821 (2006).
18. Y.-K. Sun, S. W. Cho, S. T. Myung, K. Amine, and J. Prakash, *Electrochim. Acta*, **53**, 1013 (2007).
19. S. U. Woo, C. S. Yoon, K. Amine, I. Belharouak, and Y. K. Sun, *J. Electrochem. Soc.*, **154**, A1005 (2007).
20. Y. K. Sun, S. W. Chow, S. W. Lee, C. S. Yoon, and K. Amine, *J. Electrochem. Soc.*, **154**, A168 (2007).
21. B. C. Park, H. B. Kim, S. T. Myung, K. Amine, I. Belharouak, and S. M. Lee, *J. Power Sources*, **178**, 826 (2008).
22. H. Buqa, A. Würsig, J. Vetter, M. E. Spahr, F. Krumeich, and P. Novák, *J. Power Sources*, **153**, 385 (2006).
23. M. Holzapfel, A. Würsig, W. Scheifele, J. Vetter, and P. Novák, *J. Power Sources*, **174**, 1156 (2007).
24. A. R. Armstrong, M. Holzapfel, P. Novák, C. S. Johnson, S. H. Kang, M. M.

- Thackeray, and P. G. Bruce, *J. Am. Chem. Soc.*, **128**, 8695 (2006).
25. J. Li, J. M. Zheng, and Y. Yang, *J. Electrochem. Soc.*, **154**, A427 (2007).
 26. X. J. Guo, Y. X. Li, M. Zheng, J. M. Zheng, J. Li, Z. L. Gong, and Y. Yang, *J. Power Sources*, In press. [DOI: 10.1016/j.jpowsour.2008.04.013]
 27. J. Li, W. H. Yao, and Y. Yang, *J. Phys. Chem. C*, In press. [DOI: 10.1021/jp800336n]
 28. J. S. Kim, C. S. Johnson, J. T. Vaughey, M. M. Thackeray, S. A. Hackney, W.-S. Yoon, and C. P. Grey, *Chem. Mater.*, **16**, 1996 (2004).
 29. W. S. Yoon, S. Iannopolo, C. P. Grey, D. Carlier, J. Gorman, J. Reed, and G. Ceder, *Electrochem. Solid-State Lett.*, **7**, A167 (2004).
 30. P. S. Whitfield, I. J. Davidson, P. W. Stephens, L. M. D. Cranswick, and I. P. Swainson, *Z. Kristallogr.*, **26**, 483 (2007).
 31. Z. H. Lu, and J. R. Dahn, *J. Electrochem. Soc.*, **149**, A815 (2002).
 32. F. Nobili, F. Crose, B. Scrosati, and R. Marassi, *Chem. Mater.*, **13**, 1642 (2001).
 33. Z. R. Zhang, H. S. Liu, Z. L. Gong, and Y. Yang, *J. Power Sources*, **129**, 101 (2004).
 34. Y. Kim, H. S. Kim, and S. W. Martin, *Electrochim. Acta*, **52**, 1316 (2006).
 35. Z. Chen and J. R. Dahn, *Electrochim. Acta*, **49**, 1079 (2004).
 36. Z. Chen and J. R. Dahn, *Electrochem. Solid-State Lett.*, **6**, A221 (2003).
 37. Y. K. Sun, Y. S. Lee, M. Yoshio, and K. Amine, *Electrochem. Solid-State Lett.*, **5**, A99 (2002).
 38. Y. K. Sun, K. J. Hong, J. Prakash, and K. Amine, *Electrochem. Commun.*, **4**, 344 (2002).
 39. Z. R. Zhang, H. S. Liu, Z. L. Gong, and Y. Yang, *J. Phys. Chem. B*, **108**, 17546 (2004).